Journal of System Design and Dynamics

Vol. 3, No. 3, 2009

Comparison of 2- and 3-Phase Bearingless Slice Motor Concepts*

Franz ZÜRCHER**, Thomas NUSSBAUMER***, Wolfgang GRUBER**** and Johann W. KOLAR**

E-mail: zuercher@lem.ee.ethz.ch

** ETH Zurich

*** Levitronix GmbH

**** ACCM GmbH (J. K. University Linz)

Abstract

Several processes in chemical, pharmaceutical, biotechnology and semiconductor industry require contactless levitation and rotation through a hermetically closed process chamber. A highly interesting topology for these applications is the "bearingless slice motor" concept, where already some research has been done in the past, especially focusing on topology and implementation issues. However, only little work has been done to evaluate the ideal number of motor phases. In this paper, a performance evaluation between 2-phase and 3-phase bearingless slice motor concepts is undertaken. It is shown, that 3-phase systems can supply almost the same power as state-of-the-art 2-phase systems and achieve nearly the same acceleration behavior, although they have significantly less power electronics effort.

Key words: Bearingless Motor, Magnetic Bearing, PMSM, Large Air Gap, Polyphase Motors

1. Introduction

Bearingless slice motors [1] have gained a lot of attractiveness during the last years for industry branches such as semiconductor, biotechnology and chemical industry, where spinning processes in a high-purity environment have to be performed [2],[3]. A typical configuration of the bearingless motor for these spinning applications is depicted in Fig. 1, where the levitating rotor carries a process object and is hermetically sealed in a process chamber. This encapsulation ensures a particle-free and ultra-clean environment for the process.

While three degrees of freedom (radial displacements and rotation) are controlled actively, the remaining three degrees of freedom (axial displacement and tilting) are stabilized passively by reluctance forces [1] as shown in Fig. 2. Besides the stable and vibration-free operation within the whole speed range the main challenge for these motors is to deliver a very high acceleration capability notwithstanding the large air gap in the range of several millimeters [4].

In the past, a lot of research has been done for these motors [4]-[7] in order to identify the most appropriate topology for accomplishing the required acceleration. However, little work has been done to evaluate the ideal number of motor phases, although of high importance for industrial praxis. Today's systems typically feature a two-phase bearing and a two-phase drive system powered by standard full bridges. The reason lies mainly in the fact that the two axes of the radial displacement are controlled with least effort regarding power

*Received 1 Dec., 2008 (No. 08-0834)
[DOI: 10.1299/jsdd.3.x]

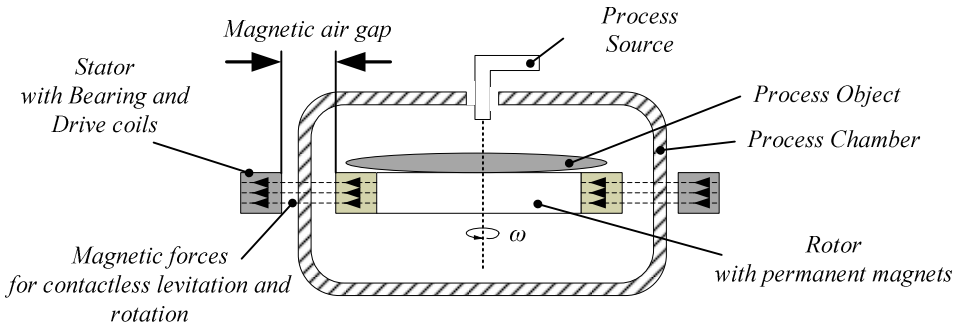

Fig. 1: Schematic view of a typical industry spinning process that is hermetically sealed with a process chamber and a magnetically levitated rotor [1].

electronics and sensors by a 2-phase bearing phase setup. In combination, typically also two drive phases (driven by full bridge topologies) are employed for generating the motor torque.

However, 3-phase configurations seem to offer an interesting alternative, since intelligent power modules [8] with integrated features (such as short-circuit protection, temperature surveillance and integrated gate drivers) can be employed and a robust and compact power electronics setup is feasible. This three-phase concept can be applied for both the bearing and the drive system of the motor.

In this paper, a performance evaluation between the two-phase and the three-phase bearingless slice motor concept is undertaken, whereby the main emphasis will be put on the performance of the drive system. The comparison is based on general analytical calculations and 3D simulation data and is exemplified for typical specifications. The findings can be used for selecting the appropriate motor and power electronics topology for future systems.

2. Motor setup

In general, many different embodiments for the stator and rotor geometries are possible for the realization of a bearingless slice motor. The key parameters to describe a specific configuration are the number of stator teeth k, the number of pole pairs of the rotor magnets p, and the number of phases for the drive windings m. Considering a certain minimum distance between the stator teeth to insert the sensors and to avoid saturation effects [9], a certain maximum number of teeth k is feasible. These k stator teeth can be used for the drive windings as well as for the bearing windings, where the sequence can be chosen arbitrarily. One tooth can even carry a combination of drive and bearing windings. For sake of simplicity and clarity this paper covers only configurations featuring one coil type per tooth with an alternating bearing-drive sequence. This typically leads to a well distributed force and torque characteristic in all directions. With this, every second tooth can be used for

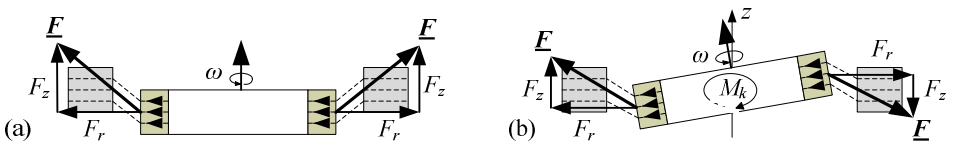

Fig. 2: (a) Axial support and (b) stabilization against tilting of the rotor by passive magnetic forces in a bearingless slice motor [1].

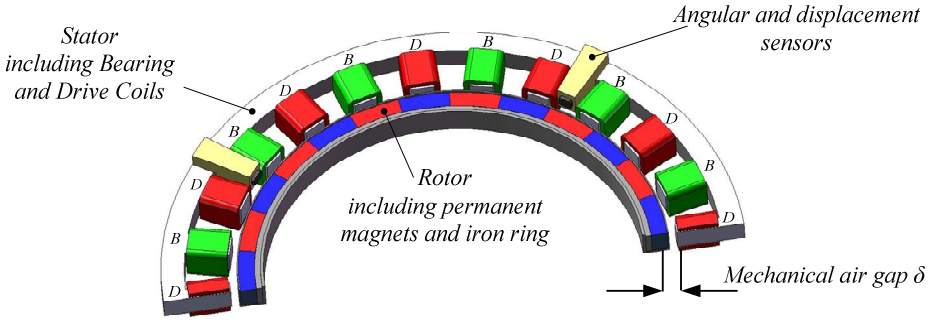

Fig. 3: Schematic cut view of the stator with alternating coils for the drive (D) and bearing (B) system and the rotor with alternately polarized permanent magnets.

the drive windings, and totally $k_D = k / 2$ teeth are available for the drive as shown in Fig. 3.

For each application, the three parameters k, p and m have to be carefully chosen in order to fulfill given requirements. As will be shown, not every possible combination of k and p is suitable for both 2-phase and 3-phase systems.

Figure 4 shows an exemplary 2-phase configuration with $k = 8$ and $p = 11$. For illustration, current is only flowing in one drive phase D_1 and in one bearing phase B_1 in positive direction generating a magnetic flux as indicated, while the currents in the other drive and bearing phases are set to zero. For the specific angular rotor position this current generates a torque M_Z in clockwise direction as well as a radial force F_X.

For a mechanical angular rotation of $90°/p$ of the rotor an analogous situation occurs for the second drive and bearing phase, generating again a torque M_Z as well as a radial force F_Y in positive y-direction.

This combination of k and p can only be used for 2-phase systems as there is no reasonable winding configuration with three phases possible. Another exemplary setup with $k = 18$ and $p = 7$ is shown in Fig. 5, where a 3-phase drive and bearing winding can be realized, but no reasonable 2-phase configuration can be found. Again, it can be seen how a positive current in the drive phase D_1 and the bearing phase B_1 generates a torque M_Z and a radial force F_X, respectively.

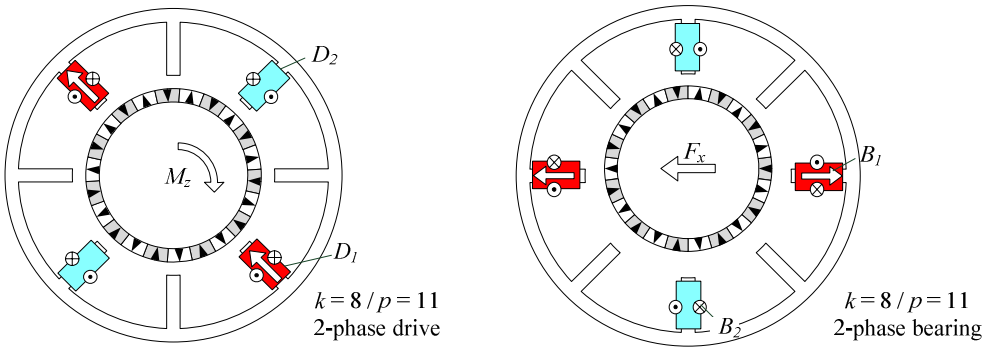

Fig. 4: Winding configuration and directions for a 2-phase system with $k = 8$ and $p = 11$. The directions of the magnetic field in case of a positive (in winding direction) current flowing in phase D_1 and B_1, respectively, are shown.

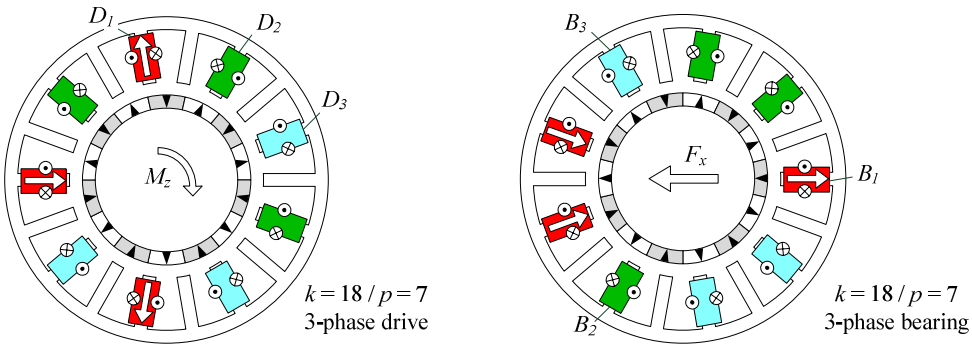

Fig. 5: Winding configuration and directions for a 3-phase system with k = 18 and p = 7. The directions of the magnetic field in case of a positive (in winding direction) current flowing in phase D_1 and B_1, respectively, are shown.

As can be seen from these two exemplary cases, the number of pole pairs p can be higher (cf. Fig. 4) or lower (cf. Fig. 5) than the number of stator teeth. Typically, good results in terms of maximum winding utilization and minimum cogging torque can be achieved, if there is neither a common divisor for k and p (for the drive system) nor for k and (p+1) (for the bearing system [1]). Otherwise, the resulting cogging torque leads to a jerky rotation at low rotational speeds.

For the experimental performance comparison (cf. section 6) of 2-phase and 3-phase systems in this paper, a design with a stator with k = 24 teeth and a rotor with p = 13 pole pairs is chosen (cf. Fig. 6). For this combination, winding configurations for the drive and bearing windings can be found for both the 2-phase and the 3-phase system (cf. Fig. 7). Calculations according to [10] and [11] show that both systems have a good winding

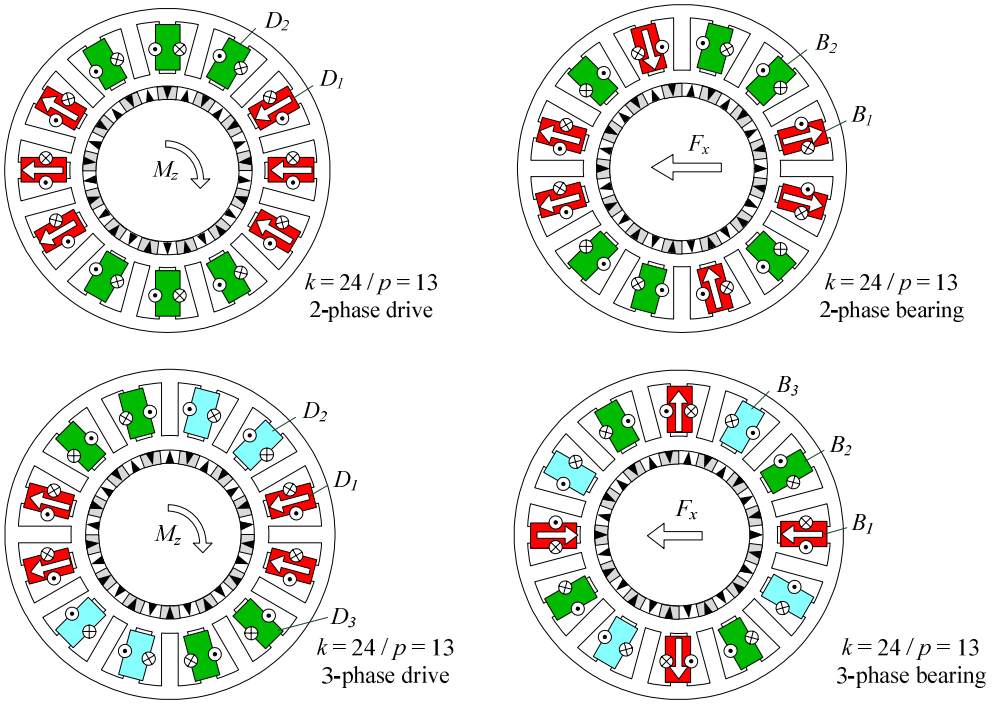

Fig. 6: 2- and 3-phase winding configuration and directions for the prototype system. The directions of the magnetic field in case of a positive (in winding direction) current flowing in phase D_1 and B_1, respectively, are shown.

utilization for the drive system, i.e., they feature a high and similar winding factor, namely $w_{2ph} = 0.90$ and $w_{3ph} = 0.95$.

In general, this is not necessarily the case, i.e., 2- and 3-phase designs may significantly differ in terms of winding utilization. Therefore, for the subsequent theoretical considerations, the winding factor will be explicitly included in the calculations in order to allow an exact comparison for any given setup.

3. Model of the drive system

In order to compare the 2-phase and the 3-phase drive system, in the following, scaling laws of the drive system are derived from a simple model. With this, the acceleration capability can be compared for the two setups. For this model, it is assumed that for both the 2-phase as well as the 3-phase configuration semiconductors with the same ampacity $I_{PE,max}$ are utilized. Furthermore, sinusoidal drive currents and voltages are assumed and saturation effects are not considered. The latter can only be neglected, if saturation effects do not influence the performance in both cases or they influence both systems in a similar way. This is not always the case for practical situations as different motor setups may show different affinity to saturation. For the chosen topology, however, both systems show very similar flux density distribution for the respective ampere-turns, whereby in both cases iron saturation can be avoided by the same stator and rotor dimensions. Fig. 7 visualizes a 3D FEM simulation result for the respective worst-case situation, where very similar maximum flux density values occur in both setups.

For the calculation of the acceleration capability mainly two parameters are crucial:

1. The induced voltage $U_{EMF,rms}$ (back EMF voltage) per phase, which is proportional to the induced voltage factor k_{EMF} per coil according to

$$U_{EMF,rms} = N_C \cdot n_R \cdot k_{EMF} \cdot w \cdot \frac{k_D}{m} \tag{1}$$

with the number of turns N_C per tooth, the rotational speed n_R in rpm, the winding factor w the number of drive teeth k_D and the number of phases m (in our case 2 and 3, respectively) of the respective setup. The factor k_{EMF} can be identified by 3D finite-element simulations of the setup and/or measured in an experimental setup.

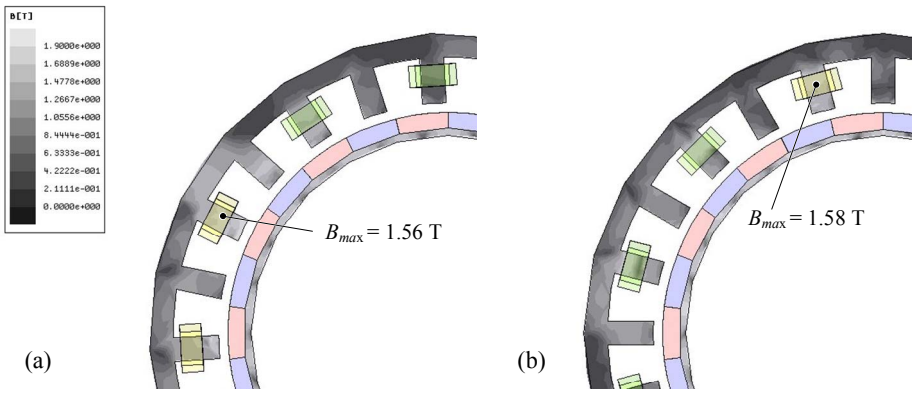

Fig. 7: Analysis of the saturation tendency of the 2-phase (a) and the 3-phase (b) motor setup with the maximum current of $I_{D,rms}$ = 15 A and the turn numbers from the experimental setup (cf. Table 1). In both cases, the respective worst-case situations (angular rotor position together with the associated ampere-turns in the phases) are shown.

2. The inductance L per phase is given by

$$L = N_C{}^2 \cdot k_L \cdot \frac{k_D}{m}, \tag{2}$$

where $1/k_L$ is the reluctance of one coil placed at one of the k_D stator teeth. Again, the parameter k_L can be identified by 3D electromagnetic simulations or measured on a practical setup.

In dependency of these two factors k_{EMF} and k_L the acceleration time to a desired rotation speed n_0 can be calculated (assuming field orientated control, i.e., induced voltage and impressed current being in phase) by

$$t_{acc} = \frac{J}{k_D \cdot k_{EMF} \cdot w \cdot N_C} \cdot \left(\frac{2\pi}{60}\right)^2 \cdot \int_0^{n_0} \frac{1}{I_{D,rms}(n_R)}\, dn_R, \tag{3}$$

whereby, neglecting coil resistance, the drive current $I_{D,rms}$ is defined by

$$I_{D,rms}(n_R) = \frac{I_{PE,\max}}{\sqrt{2}} \quad for \quad \sqrt{2} \cdot I_{D,rms} > I_{PE,\max} \tag{4}$$

and

$$I_{D,rms}(n_R) = \frac{60}{2\pi \cdot n_R \cdot p \cdot L} \frac{\sqrt{U_{D,rms}^2 - U_{EMF,rms}^2}}{} \quad for \quad \sqrt{2} \cdot I_{D,rms} < I_{PE,\max} \tag{5}$$

with the maximum allowable power electronics current $I_{PE,max}$ and the specific applicable drive voltage $U_{D,rms}$. This correlation is illustrated in Fig. 8. That means that above a certain rotational speed n_C the drive current (and thus the torque) is reduced due to the influence of the coil inductance L (cf. Fig. 8) and the back EMF voltage.

If the number of coil windings is reduced in order to shift n_C up towards higher speeds (probably out of the operating speed range as it is the case for N_C = 45 in Fig. 8) and to maximize the drive current $I_{D,rms}$, the induced voltage $U_{EMF,rms}$ is reduced according to (1). Apparently, a minimum acceleration time is achieved by a compromise between high number of turns (high power at low speeds) and a low number of turns (high power at high speeds). Hence, the number of turns can be optimized for each configuration depending on the ratio between the factors k_{EMF} and k_L for a certain required rotation speed n_0.

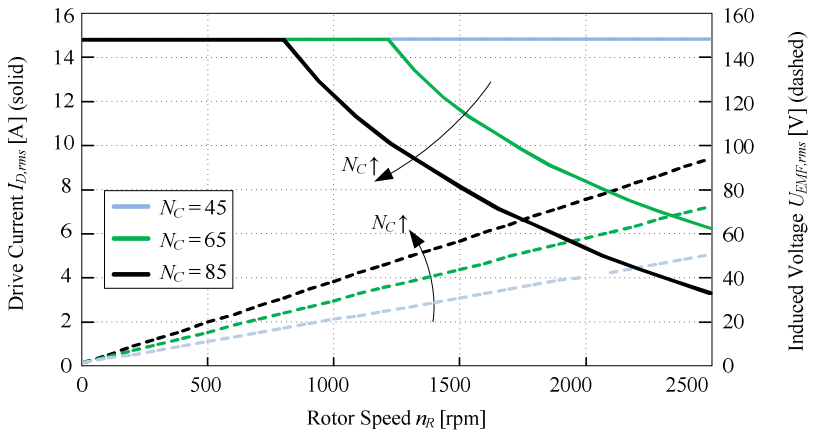

Fig 8: Calculated drive current $I_{D,rms}$ (solid line) and induced voltage $U_{EMF,rms}$ (dashed line) in dependency of the rotor speed n_R for U_{DC} = 300V and $I_{PE,max} = \sqrt{2} \cdot 15$A.

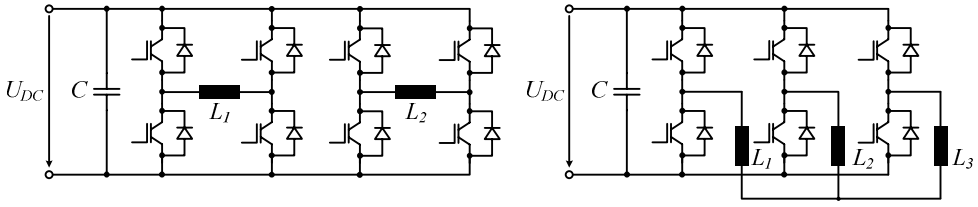

(a) (b)

Fig. 9: Power electronics inverter topology for the 2-phase (drive or bearing) system (a) with two full-bridges and for the 3-phase system (b) with three half-bridges in star connection.

4. Power electronics setup

As mentioned in the introduction, bearingless motors typically use 2-phase winding setups for both the drive and the bearing system. Each phase is then usually driven by a full-bridge inverter circuit as shown in Fig. 9(a). Alternatively, a 3-phase configuration is possible, with the three phases being connected in star for both the drive and the bearing system, as shown in Fig. 9(b). In this paper, only these two power electronic topologies are considered, although different power electronics topologies for 2-phase and 3-phase configurations would be possible.

For the comparison of the power electronics effort of the two different setups, a component load factor *CLF* as introduced in [12] is defined, which can be used as an approximate measure for the total power electronics size, losses, and cost. The component load factor can be calculated according to

$$CLF = n \cdot I_{rms} \cdot U_{DC}\,, \tag{6}$$

where n is the number of transistors, U_{DC} the dc link voltage, and I_{rms} is the maximum allowable rms current per transistor.

For the two chosen setups, the power electronics for the 2-phase system is apparently characterized by a higher number n of required semiconductors than for the 3-phase system. In the latter case, there are only three half-bridges needed due to the star-connection of the three phases, whereas two full-bridges are required for the 2-phase system, which correspond to four half-bridges. Hence, a factor ξ_{CLF} describing the power electronics effort ratio can be defined by the ratio of the two component load factors

$$\xi_{CLF} = \frac{CLF_{3\,ph}}{CLF_{2\,ph}} = \frac{n_{3\,ph}}{n_{2\,ph}} = 0.75\,, \tag{7}$$

since both the allowable current I_{rms} of each transistor and the dc link voltage U_{DC} are assumed to be the same for both topologies.[1]

However, the ratio of the power being delivered to the phases (assuming again the same ampacity of the power semiconductors) is different from this value. In the case of a full-bridge configuration as it is the case for the 2-phase system the available drive voltage $U_{D,rms}$ is given by

[1] A change of the current or the voltage rating for one of the two setups would obviously change the ratio in (7), but would also change the ratio of the delivered power according to (12) likewise, such that the relation of power electronics effort and performance maintains the same. Analogously, also other power electronics topologies, e.g. three full-bridges for the 3-phase setup, would lead to both an increase of the power electronics effort index (7) and the performance index (12).

$$U_{D,rms} = \frac{U_{dc}}{\sqrt{2}} \tag{8}$$

and in the case of a three-phase star-connection

$$U_{D,rms} = \frac{U_{dc}}{\sqrt{6}}\,. \tag{9}$$

Thus, the voltage $U_{D,rms}$ over each of the drive coils is lower in the case of the 3-phase star-connection, as can be seen by comparing (7) and (8). In return, in case of the 3-phase concept one more phase contributes to the drive power. The total power of the 2-phase system is therefore given by

$$P_{2ph} = 2 \cdot U_{D,rms} \cdot I_{D,rms} = I_{D,rms} \frac{2}{\sqrt{2}} \cdot U_{dc} \tag{10}$$

and in the case of the 3-phase system by

$$P_{3ph} = 3 \cdot U_{D,rms} \cdot I_{D,rms} = I_{D,rms} \frac{3}{\sqrt{6}} \cdot U_{dc}\,. \tag{11}$$

With this, a power ratio ξ_P can be calculated as the ratio of the deliverable power value of the 3-phase to the 2-phase system:

$$\xi_P = \frac{P_{3ph}}{P_{2ph}} = \frac{\sqrt{3}}{2} = 0.87\,. \tag{12}$$

Thus, the 3-phase configuration delivers 13% less drive power compared to the 2-phase full-bridge configuration (while having 25% less power electronics effort). However, for comparing the total drive performance of the two setups, the acceleration behavior over a certain specified rotational speed range has to be considered. This will be carried out in the subsequent section based on the model of the drive system that has been derived before.

5. Performance comparison

In order to compare the drive performance of the 3-phase and the 2-phase setup, an acceleration performance factor is introduced:

$$\xi_A = \frac{1/t_{3ph}}{1/t_{2ph}} = \frac{t_{2ph}}{t_{3ph}}\,. \tag{13}$$

As concluded before, the achievable acceleration time to a certain required rotational speed n_0 strongly depends on the selected number of drive turns N_C. Based on (1) to (5), for specific values of the induced voltage factor k_{EMF}, the coil inductance factor k_L, the number of phases m, the applicable drive voltage $U_{D,rms}$, the required rotation speed n_0, the number of pole pairs p, and the maximum allowable current $I_{PE,max}$ always an optimum number of drive turns $N_{C,opt}$ can be found. Now, the question arises, if this optimum number of turns automatically leads to an acceleration performance factor ξ_A being equal to the power ratio ξ_P.

As a detailed analysis shows, only the ratio k_L / k_{EMF} is of importance for the acceleration factor ξ_A. Figure 10 shows that for small values of the ratio the factor ξ_A is essentially identical with ξ_P = 0.87. This is due to the fact that the inductance value is very small

(resulting in a very steep decay of the drive current above n_C) so that the optimization of the number of turns leads to $n_0 = n_C$ and the maximum current can be driven over the whole speed range.

For higher ratios of k_L / k_{EMF} the before-mentioned trade-off between high power at low speeds (high number of turns) and high power at high speeds (high number of turns) occurs. As can be seen in Fig. 10, this causes an increase of the acceleration factor ξ_A for the case $w_{3ph} / w_{2ph} \geq 1$, i.e., a relative improvement of the 3-phase setup compared with the 2-phase setup. In contrary, ξ_A may decrease for $w_{3ph} / w_{2ph} < 1$. In Fig. 10, the acceleration ratio is plotted for winding factor ratios in the range of $w_{3ph} / w_{2ph} = 0.8 \ldots 1.2$.

The typical ratio of k_L / k_{EMF} for bearingless motors with large air gaps lies in the range of 0.05 … 0.15 mH·rpm/V, resulting in $\xi_A = 0.89 \ldots 0.92$. With this, the star-connected 3-phase setup has about only 10% lower acceleration performance compared to the full-bridge 2-phase system, even though the power electronics effort is only 75%.

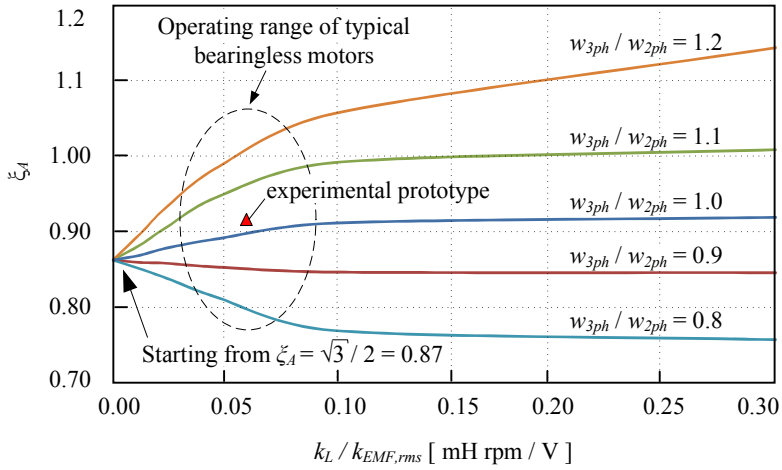

Fig 10: Acceleration performance factor ξ_A in dependency on the ratio of $k_L / k_{EMF,rms}$.

6. Experimental verification

In order to verify the analytical considerations, a prototype has been designed and built, which allows to implement both 2-phase and 3-phase winding configurations. As previously mentioned, $k = 24$ stator claws and $p = 13$ pole pairs have been chosen with the drive winding factors $w_{2ph} = 0.9$ and $w_{3ph} = 0.95$. A photograph of the prototype system is shown

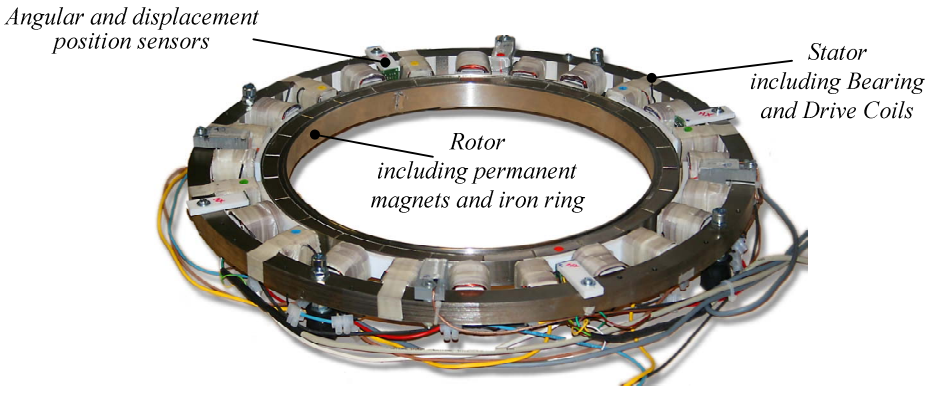

Fig. 11: Prototype featuring $k = 24$ stator teeth and a rotor with $p = 13$ pole pairs.

in Fig. 11 and characteristic key data is compiled in Table 1. Fig. 12 shows exemplarily the measurements of the 3-phase system during acceleration from 0 rpm to 1500 rpm. The acceleration times of different run-ups up to the specified maximum speed n_0 = 2500 rpm for both systems (2-phase and 3-phase) are depicted in Fig. 13. It can be seen, that they achieve basically similar acceleration times. The acceleration performance factor ξ_A according to (12) can be calculated for the maximum speed (n_0 = 2500 rpm) to ξ_A = 0.91, which is in good accordance to the analytically calculated value indicated in Fig. 10 for the given value of k_L / k_{EMF} = 0.065 mH rpm/V.

7. Conclusion

This paper shows that 3-phase drive winding concepts may offer a good alternative to the conventionally used 2-phase concepts for bearingless motors. Although they have significantly less power electronics effort and offer the possibility to employ commercially available and highly compact intelligent power modules, they feature only a slightly lower

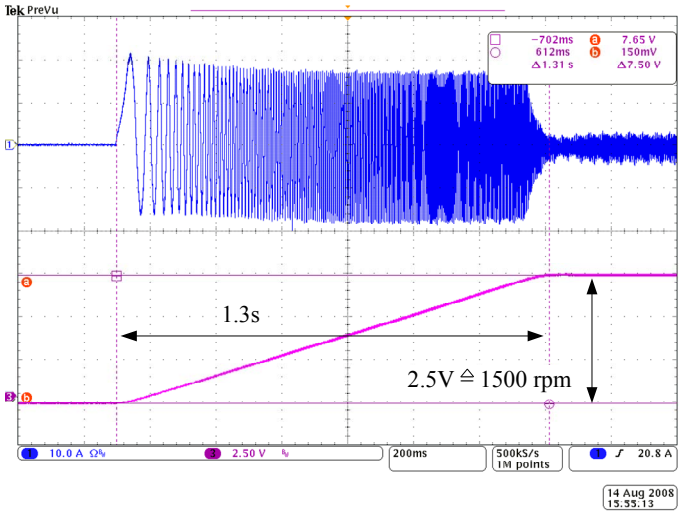

Fig. 12: Exemplary measurement of the current in one of three drive phases during acceleration from 0 rpm to 1500 rpm with the 3-phase system.

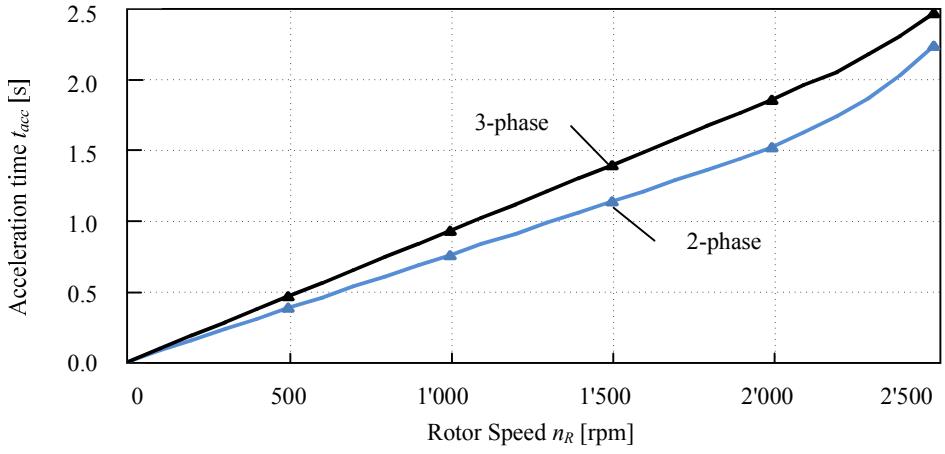

Fig. 13: Acceleration performance results for the bearingless slice motor at hand with a 2-phase drive windings configuration compared to the same system with a 3-phase drive windings configuration. Each measurement point indicates the needed acceleration time from 0 rpm to the specified speed up to 2500 rpm.

acceleration performance than 2-phase setups. These findings can be used for further designs of bearingless slice motors.

TABLE 1: Design data of the experimental setup

Total Number of stator teeth	k	24	
Number of drive teeth	k_D	12	
Number of bearing teeth	k_B	12	
Number of pole pairs	p	13	
Stator outer diameter	D	500	mm
Mechanical air gap	δ	7	mm
Rotor weight	m	3.1	kg
Radial stiffness	k_R	-95.3	N/mm
Axial stiffness	k_Z	20.0	N/mm
Force-current factor	k_I	18.5	mN/(AWdg)
Inductivity factor per coil	k_L	209.2	nH/Wdg^2
Voltage-speed factor	k_{EMF}	3.2	mVrms/(Wdg·rpm)
2-phase system			
Bearing phase winding number	N_B	12 x 65	turns
Drive phase winding numbers	N_D	12 x 55	turns
3-phase system			
Bearing phase winding number	N_B	12 x 65	turns
Drive phase winding numbers	N_D	12 x 45	turns

References

[1] R. Schoeb, N. Barletta, "Principle and application of a bearingless slice motor", Proc. 5th Int. Symposium on Magnetic Bearings (ISMB5), Kanazawa (Japan), pp. 313-318, 1996.

[2] Y. Chisti, M. Moo-Young, "Clean-in-place systems for industrial bioreactors: Design, validation and operation," *Journal of Industrial Microbiology and Biotechnology*, 1994.

[3] J. Boehm, R. Gerber, J.R. Hartley, S. Whitley, "Development of active magnetic bearings for high speed rotors," *IEEE Trans. on Magnetics*, vol.26, no.5, pp.2544-2546, Sep. 1990.

[4] P. Karutz, T. Nussbaumer, W. Gruber, J.W. Kolar, "The bearingless 2-level motor", Proc. 7th Int. Conf. Power Electron. and Drive Systems (PEDS'07), Bangkok, Thailand, Nov. 27-30, 2007.

[5] S. Silber, W. Amrhein, P. Boesch, R. Schoeb, N. Barletta, "Design aspects of bearingless slice motors", IEEE Trans. Mechatron., vol. 10, no. 6, pp. 611-617, Dec. 2005.

[6] J. Amemiya, A. Chiba, D.G. Dorrell, T. Fukao, "Basic characteristics of a consequent-pole-type bearingless motor", IEEE Trans. Magn., vol. 41, no. 1, pp. 82-89, Jan. 2005.

[7] T. Schneeberger, J.W. Kolar, "Novel integrated bearingless hollow-shaft drive", Proc. 41st IEEE Ind. Appl. Conf. (IAS'06), Tampa, USA, Oct. 8-12, 2006.

[8] International Rectifier: Integrated Hybrid IC IRAMY30UP60B, Datasheet (2006).

[9] P. Karutz, T. Nussbaumer, W. Gruber, J.W. Kolar, "Saturation effects in high acceleration bearingless slice motors", Proc. Int. Symp. Ind. Electron. (ISIE'08), Cambridge, UK, Jun. 30 – Jul. 2, 2008.

[10] F. Magnussen, C. Sadarangani, "Winding factors and Joule losses of permanent magnet machines with concentrated windings", Electric Machines and Drives Conference (IEMDC'03.), June 1-4, 2003.

[11] D. Zhu; X. Qiu; N. Zhou; Y. Yan, "A comparative study of winding factors between distributed windings and non-overlapping concentrated windings", Third International Conference on Electric Utility Deregulation and Restructuring and Power Technologies (DRPT 2008), April 6-9, 2008.

[12] B. Carston, "Converter Component Load Factors; A Performance Limitation of Various Topologies", PCI '88 Munich, W. Germany, Dec. 1988.